Control Parameters Design Procedure for Multi-converters DC Power System Considering Dynamic Interaction Between Converters

Xueshen Zhao, Lin Zhu, Li Guo, Xialin Li, Zhi Wang, Hao Lu, *Member*, *IEEE*, and Chengshan Wang, *Senior Member*, *IEEE*

***Abstract*—Due to dynamic interaction between converters, design of control parameters of multi-converters medium-voltage DC (MVDC) power system is much more complicated than of a single-converter situation. Open-loop and closed-loop transfer functions considering control-loops dynamic interaction between converters are developed, which are suitable for studying influence of control parameters on system stability. With the above transfer functions, a system-level control parameter design procedure for dynamic stability (e.g., oscillation frequency and damping factor) of system is proposed. If there are many converters, computational burden of system-level control parameters design procedure will be huge. For this reason, a control parameter sharing method is further proposed in this paper, which is based on dynamic interaction mechanism between converters. In this sharing method, control parameters of equivalent reduced-order model of the system are shared with each converter, so calculation burden of control parameters of system is reduced significantly. Consequently, dynamic stability of the system can be designed by equivalent reduced-order model. Experiments are conduced to validate the system-level control parameter design procedure.**

***Index Terms*—Control parameters design procedure, dynamic interaction, medium-voltage DC (MVDC) power system, sharing principle.**

I. Introduction

THE zero carbon transformation of energy system requires development of renewable energy, such as photovoltaic, wind turbine, fuel cell, and so on [1], [2]. Medium-voltage DC (MVDC) power system has become an effective solution with high penetration of renewable energy [3]. In multi-converters MVDC power system, stability is the most significant research due to negative incremental resistance of constant power load (CPL) and unexpected dynamic interaction between converters. Dynamic stability of system can be guaranteed based on appropriate control parameters [4]. But design complexity of control parameters of the system is huge. This is because change of control parameters of one converter can also greatly affect other converters' behavior due to existing dynamic interactions between converters [5]. Therefore, how to design controller parameters of the system exactly needs to be further investigated.

With open-loop and closed-loop transfer functions, control parameters of a single-converter are usually designed in frequency domain. Control parameters of each converter in a DC system are individually designed with an acceptable stability margin in [6] and [7]. However, transfer functions in [6] and [7] are developed based on converters controlled by voltage single-loop control. In [8], a detailed controller parameter design procedure is proposed, which is suitable for converters with conventional voltage and current double-loop control. However, design procedures in [8] and [9] do not consider type of load. In [10], a detailed controller parameter design procedure, how to achieve expected dynamic performance of converter with resistive load, is introduced in detail. But negative resistance characteristics of CPLs are not considered. Literature [11] investigates effect of control-loops interactions on power stability limits of a voltage-source converter (VSC). In addition, above transfer functions are all established based on single-converter situation, which cannot reflect dynamic interaction between converters in multi-converters DC system [12]. In literature [13], a second-order generalized model is proposed to simplify design of control parameters and stability analysis of an N-phase interleaves boost converter system. However, this system in [13] is controlled by the proposed sliding-mode control rather than widely used voltage-current double-loop control. With the proposed self-impact components and interaction-impact components, influence of interactions of VSCs on DC voltage stability can be effectively studied by [14]. However, control parameters are difficult to be designed quantitatively by closed-loop Multi-VSCs model in [14]. So, how to establish the open-loop and closed-loop transfer functions of each control loop, which are suitable for design of control parameters from the perspective of system-level stability, is still an unsolved problem?

In numerous research results, stability dynamics of DC systems may be in a wide range of oscillation frequencies (e.g., 10–40 Hz) [15]–[17]. A generic small signal mathematical model of DC system was developed by [18], which can

Manuscript received January 26, 2022; revised April 7, 2022; accepted May 10, 2022. Date of online publication December 28, 2023; Date of current version April 22, 2024. This work was supported in part by the National Key Research and Development Program of China under Grant 2020YFB1506800, in part by the China Postdoctoral Science Foundation under Grant 2021M692378, and in part by the National Natural Science Foundation of China under Grant 51977142.

X. S. Zhao, L. Zhu (corresponding author, email: lin_zhu@tju.edu.cn), L. Guo, X. L. Li, Z. Wang, H. Lu and C. S. Wang are with the Key Laboratory of Smart Grid of Ministry of Education, Tianjin University, Tianjin 300072, China.

DOI: 10.17775/CSEEJPES.2022.00620

facilitate quantitative calculation of voltage control parameters of multiple converters. For a single-bus DC system, its equivalent RLC circuit model can be constructed by [19] neglecting current control parameters. In addition, a generic reduced-order modeling method suitable for two different droop control modes was proposed by [20], which can be used to explore dynamic stability of DC voltage around 5 Hz. Thus, models of [18]–[20] can provide theoretical basis for optimization of voltage control parameters, but not for current control parameters. As found in [21], dominant low-frequency (LF) response of a typical single-bus DC microgrids is mainly determined by droop controller of voltage-controlled (VC) distributed generations(DGs). Based on this finding, a simplified equivalent model is proposed for LF stability analysis of each single-bus DC microgrid. Considering the impedance model of interconnected lines, effect of droop control parameters on LF stability (around 33 Hz) of multi-bus DC microgrids can also be investigated. However, VC-DG in [21] is controlled by droop-based voltage single-loop instead of most commonly used droop-based voltage-current double-loop. Based on design procedure proposed in [22], control parameters of single-bus multi-converters DC system can be quantitatively calculated. For those nonlinear control methods in [23], [24], control parameters usually need to be tuned based on many simulation results. Then, for two DC systems aggregated by different circuit parameters, it is not easy to achieve desired dynamic performance (e.g., small overshoot, less oscillations, and small settling time) by relying only on control parameter tuning experience in [23], [24]. In summary, for precise design needs of DC systems with stable dynamics over a wide range of oscillation frequencies (e.g., 10–40 Hz) [15]–[17], corresponding general control parameter design methods have not been reported.

It is well known, due to dynamic interaction between converters, expected dynamic stability of multi-converters MVDC power system is difficult to be designed qualitatively and quantitatively [24]. Therefore, it is urgent to establish open-loop and closed-loop transfer functions considering dynamic interaction between converters. In addition, system-level control parameters design procedure is also essential. Major contributions of this work can be drawn as:

1) To evaluate system stability as influenced by control parameters, open-loop and closed-loop transfer functions considering control-loops dynamic interaction between converters are established. In addition, number of poles (or zeros) of transfer function considering dynamic interaction between converters is very consistent with single-converter situation.

2) With the above transfer functions considering dynamic interaction between converters, a system-level control parameter design procedure is proposed. In this design procedure, control parameters (e.g., state feedback control, current control, voltage control, and etc.) of all converters are designed from the perspective of system dynamic stability. Through mutual cancellation of some zeros and poles, the system can be designed as a second-order model. Then, analytical solutions of dynamic stability (e.g., oscillation frequency and damping factor) can be obtained.

3) According to dynamic interaction mechanism between converters of each control loop in the system, a control parameter sharing method is proposed. With this sharing method, control parameters of equivalent reduced-order model of the system are shared with each converter.

The rest of the paper is organized as follows. In Section II, open-loop and closed-loop transfer functions considering dynamic interaction between converters are established, and system-level design procedure of the system are introduced in detail. Control parameter sharing method is proposed in Section III. Detailed dynamic stability analysis and experimental verifications are provided in Section IV. Section V concludes the paper.

II. A System-level Control Parameters Design Procedure Considering the Dynamic Interaction between Converters

Topology of considered multi-converters medium-voltage DC (MVDC) power system are depicted in Fig. 1(a): n line regulating converters (LRCs) and m constant power loads (CPLs).

In this section, open-loop and closed-loop transfer functions of converter are established, which considers dynamic interaction between converters. In addition, a system-level control parameters design procedure is proposed, which is divided into four steps to control parameters of the system, as shown in Fig. 2(a).

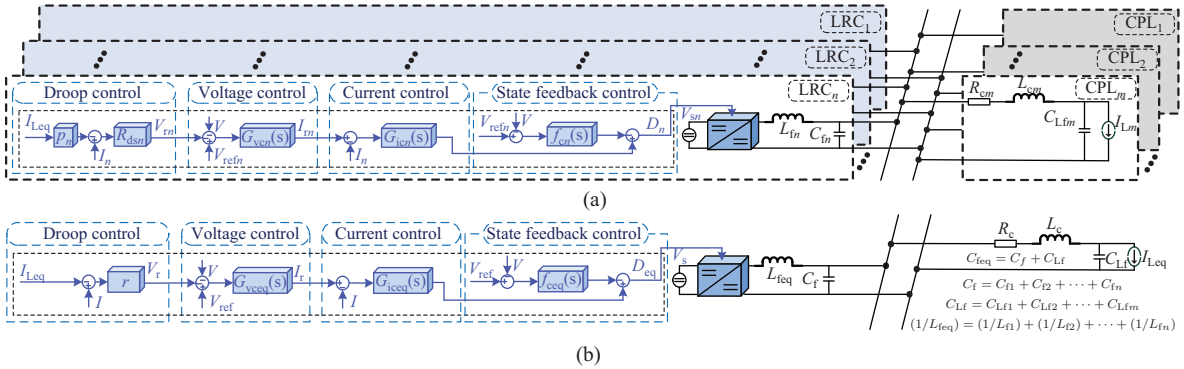

Fig. 1. Topology of the tested DC system. (a) Multi-converters MVDC power system. (b) Equivalent reduced-order model (single-converter).

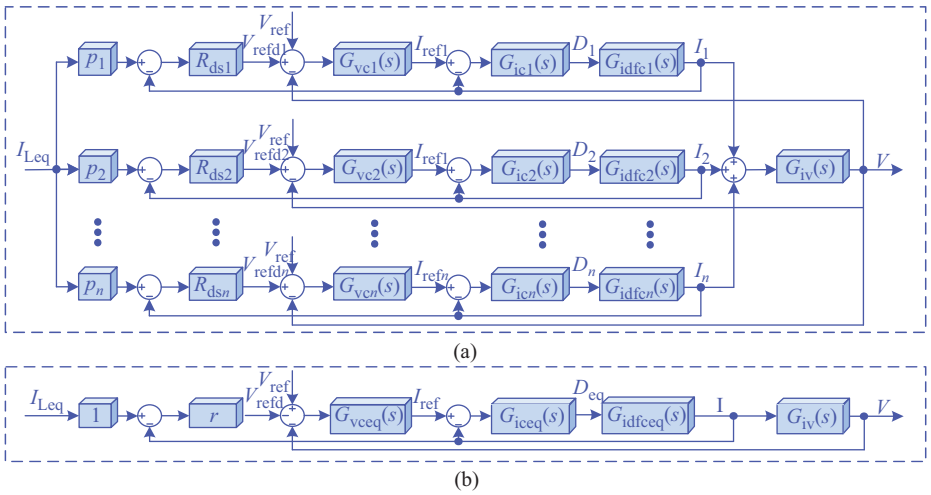

Fig. 2. Control architecture of the tested DC system. (a) Multi-converters MVDC power system. (b) Equivalent reduced-order model.

A. Design of State Feedback Control Parameters

1) Transfer Function of State Feedback Control Considering Dynamic Interaction between Converters

When influence of cable can be ignored in Fig. 1(a), the control-to-output transfer function $G_{\mathrm{vd}k}(s)$ of k^{th} LRC can be written as:

$$G_{\mathrm{vd}k}(s)=\left(\frac{V_{sk}}{C_{\mathrm{eq}}L_{\mathrm{f}k}}\right)\frac{1}{s^2-\frac{1}{R_{\mathrm{eq}}C_{\mathrm{eq}}}s+\frac{1}{L_{\mathrm{eq}}C_{\mathrm{eq}}}} \tag{1}$$

where V_{sk} and $L_{\mathrm{f}k}$ are input voltage and output filter inductor of k^{th} LRC respectively, $(k=1,2,\cdots,n)$, C_{eq} and L_{eq} are equivalent filter capacitor and inductor respectively, R_{eq} is equivalent resistor of all CPLs [3]. From (1), it can be concluded transfer function $G_{\mathrm{vd}k}(s)$ includes filter parameters of k^{th} LRC itself, as well as those of other converters. In addition, number of poles (or zeros) of transfer function $G_{\mathrm{vd}k}(s)$ is very consistent with single-converter situation detailed in [10], as shown in Table I.

TABLE I
THE NUMBER OF ZEROS AND POLES OF THE TRANSFER FUNCTIONS

Control loop	Transfer function	The number of zeros	The number of poles
State feedback control	$G_{\mathrm{vd}k}(s)$	0	2
	$G_{\mathrm{idfc}k}(s)$	1	2
Current control	$T_{\mathrm{iifc}k}(s)$	2	3
	$G_{\mathrm{iifc}k}(s)$	2	3
Voltage control	$G_{\mathrm{ivd}k}(s)$	1	3
	$T_{\mathrm{vivfc}k}(s)$	2	4
	$G_{\mathrm{vivfc}k}(s)$	2	4
Droop control	$G_{\mathrm{vivrfc}k}(s)$	2	4

From (1), it can be concluded transfer function $G_{\mathrm{vd}k}(s)$ with CPL load is unstable. Then, a state feedback control method is introduced by [3], as shown below.

$$f_{ck}(s)=(K_{1k}+K_{2k}s) \tag{2}$$

where K_{1k} and K_{2k} are proportional and derivative feedback control gains of state feedback control $f_{ck}(s)$ respectively, V is DC bus voltage. Considering state feedback control $f_{ck}(s)$, then control-to-inductor current transfer function $G_{\mathrm{idfc}k}(s)$ of k^{th} LRC can be written as:

$$G_{\mathrm{idfc}k}(s)=\frac{\frac{V_{sk}G_{\mathrm{iv}}(s)}{L_{\mathrm{f}k}C_{\mathrm{eq}}}}{s^2+\left(\left(\sum_{x=1}^{n}\frac{K_{2x}V_{sk}}{C_{\mathrm{eq}}L_{\mathrm{f}k}}\right)-\frac{1}{R_{\mathrm{eq}}C_{\mathrm{eq}}}\right)s+\left(\sum_{x=1}^{n}\frac{K_{1x}V_{sk}}{C_{\mathrm{eq}}L_{\mathrm{f}k}}\right)+\frac{1}{L_{\mathrm{eq}}C_{\mathrm{eq}}}} \tag{3}$$

where p_k is load sharing coefficient ($\sum p_k=1$) of k^{th} LRC, and $G_{\mathrm{iv}}(s)$ is defined as $(C_{\mathrm{eq}}s-1/R_{\mathrm{eq}})$.

2) Design of State Feedback Control Parameters Considering Dynamic Interaction between Converters

Equivalent filter inductor L_{eq} is system-level result of dynamic interaction of filter inductors between converters. Similarly, dynamic interaction of filter capacitors between converters also exits, which is the reason why equivalent filter capacitor C_{eq} can be obtained. According to dynamic interaction of state feedback control between converters, the characteristic equation of (3) can be established. The characteristic equation of (3) can be written in the form of a second-order model with a natural angular frequency ω_{feq} and damping factor ζ_{feq}. To have larger damping, ζ_{feq} can be selected as 0.7. While design of ω_{feq} should be smaller than current controller bandwidth. It is assumed state feedback control parameters are very consistent for each converter, i.e. $K_{1k}=K_{1(k+1)}$, and $K_{2k}=K_{2(k+1)}$. Then, state feedback control parameters for each converter will be calculated by solving the characteristic equation of (3).

B. Design of Current Control Parameters

1) Transfer Function of Current Control Considering Dynamic Interaction between Converters

As shown in Fig. 1(a), current controller $G_{\mathrm{ic}k}(s)$ of k^{th} LRC can be written as:

$$G_{\mathrm{ic}k}(s)=k_{\mathrm{pi}k}+\frac{k_{\mathrm{ii}k}}{s}=k_{\mathrm{pi}k}\left(1+\frac{\eta_{\mathrm{i}k}\omega_{ick}}{s}\right) \tag{4}$$

where $k_{\mathrm{pi}k}$ and $k_{\mathrm{ii}k}$ are proportional and integral gains of current controller $G_{\mathrm{ic}k}(s)$ of k^{th} LRC, respectively. It is assumed $\omega_{\mathrm{ic}k}$ is the crossover frequency of current control loop

of k^{th} LRC, and $\eta_{\text{i}k}$ is defined as ratio of $k_{\text{ii}k}$ to $(\omega_{\text{ic}k} \times k_{\text{pi}k})$. Loop gain $T_{\text{iifc}k}(s)$ and closed-loop transfer function $G_{\text{iifc}k}(s)$ of current control of k^{th} LRC can be obtained, as shown in (5) and (6), respectively.

$$T_{\text{iifc}k}(s) = G_{\text{idfc}k}(s)G_{\text{ic}k}(s) \tag{5}$$

$$G_{\text{iifc}k}(s) = \frac{G_{\text{vd}k}(s)G_{\text{ic}k}(s)G_{\text{iv}}(s)}{\left\{ \begin{array}{c} (1+\sum_{x=1}^{n}\{(K_{1x}+K_{2x}s)G_{\text{vd}x}(s)\}) \\ +G_{\text{vd}k}(s)G_{\text{ic}k}(s)G_{\text{iv}}(s) \end{array} \right\}} \tag{6}$$

Unlike literature [10], transfer function $G_{\text{iifc}k}(s)$ of k^{th} LRC takes into account not only its own parameters but also those of other LRCs. Then, dynamic interaction of current control between converters can be revealed intuitively by (6).

2) Design of Current Control Parameters Considering Dynamic Interaction between Converters

Taking dynamic interaction of state feedback control between converters into account, transfer function $G_{\text{idfc}k}(s)$ can be constructed. Further, current control parameters can be designed with predetermined crossover frequency $\omega_{\text{ic}k}$ and $\eta_{\text{i}k}$. It is suggested current control parameters of each converter in the system should be designed sequentially: first, 1^{th} LRC, then 2^{th} LRC, and finally n^{th} LRC. Taking k^{th} LRC as an example, recommended design procedure of its current control parameters is introduced in detail. Considering expected dynamic performance and sufficient stability margin, crossover frequency can be chosen as one tenth of switching frequency $f_{\text{s}k}$ of the k^{th} LRC, and $\eta_{\text{i}k}$ can be selected as 0.1.

C. Design of Voltage Control Parameters

1) Transfer Function of Voltage Control Considering Dynamic Interaction between Converters

Voltage open-loop transfer function $G_{\text{ivd}k}(s)$ of k^{th} LRC can be written as:

$$G_{\text{ivdfc}k}(s) = \frac{G_{\text{iifc}k}(s)}{p_k G_{\text{iv}}(s)} \tag{7}$$

As shown in Fig. 1(a), voltage controller $G_{\text{vc}k}(s)$ of k^{th} LRC can be written as:

$$G_{\text{vc}k}(s) = k_{\text{pv}k} + \frac{k_{\text{iv}k}}{s} = k_{\text{pv}k}\left(1 + \frac{\omega_{\text{vL}k}}{s}\right) \tag{8}$$

where $k_{\text{pv}k}$ and $k_{\text{iv}k}$ are proportional and integral gains of voltage controller $G_{\text{vc}k}(s)$ of k^{th} LRC, respectively. It is assumed $\omega_{\text{vc}k}$ is crossover frequency of voltage control loop of k^{th} LRC, and $\eta_{\text{v}k}$ is defined as ratio of $k_{\text{iv}k}$ to $(\omega_{\text{vc}k} \times k_{\text{pv}k})$. Loop gain $T_{\text{vivfc}k}(s)$ and closed-loop transfer function $G_{\text{vivfc}k}(s)$ of voltage control of k^{th} LRC can be obtained, as shown in (9) and (10), respectively.

$$T_{\text{vivfc}k}(s) = G_{\text{ivdfc}k}(s)G_{\text{vc}k}(s) \tag{9}$$

$$G_{\text{vivfc}k}(s) = \frac{G_{\text{vd}k}(s)G_{\text{ic}k}(s)G_{\text{vc}k}(s)}{\left\{ \begin{array}{c} \sum_{x=1}^{n}\{G_{\text{vd}x}(s)G_{\text{ic}x}(s)(G_{\text{vc}x}(s)+p_x G_{\text{iv}}(s))\} \\ +\sum_{x=1}^{n}\{(K_{1x}+K_{2x}s)G_{\text{vd}x}(s)\}+1 \end{array} \right\}} \tag{10}$$

From (10), it is clear parameters of k^{th} LRC and other LRCs are considered by transfer function $G_{\text{vivfc}k}(s)$. Different with transfer function applied to a single-converter situation in [10], dynamic interaction of voltage control between converters can be directly reflected by transfer function $G_{\text{vivfc}k}(s)$.

2) Design of Voltage Control Parameters Considering Dynamic Interaction between Converters

Voltage control parameters of each converter in the system can be designed according to procedure similar to current control. Considering dynamic interaction of current control between converters, transfer function $G_{\text{ivd}k}(s)$ can be given. Then, based on frequency domain curves (e.g. crossover frequency and phase margin) of transfer function $T_{\text{vivfc}k}(s)$, the voltage control parameters can be designed separately based on preset $\omega_{\text{vc}k}$ and $\eta_{\text{v}k}$. In order to realize mutual cancellation of some zeros and poles, crossover frequency $\omega_{\text{vc}k}$ can be selected as $0.1 \sim 0.3$ times $\omega_{\text{ic}k}$, and $\eta_{\text{v}k}$ can be selected as $0.1 \sim 5$. With the characteristic equation of transfer function $G_{\text{vivfc}k}(s)$, a system-level equivalent voltage controller $G_{\text{vceq}}(s)$ can be built from dynamic interaction of voltage controllers $G_{\text{vc}k}(s)$ between converters. If voltage control parameters of all converters are tuned according to the same design principle (e.g., $\omega_{\text{vc}k} = 0.1 \times \omega_{\text{ic}k}$, and $\eta_{\text{v}k} = 0.1$), then all voltage controllers have the same zero of $0.01 \times \omega_{\text{ic}k}$. Conversely, zeros will be different among voltage controllers. In any case, all zeros of all voltage controllers $G_{\text{vc}k}(s)$ in DC system can be equivalent to one zero of equivalent voltage controller $G_{\text{vceq}}(s)$. Since number of zeros and poles of transfer function $G_{\text{vivfc}k}(s)$ is 2 and 4, respectively, the design burden of suitable voltage control parameters can be significantly reduced.

D. Design of Droop Control Parameters

1) Transfer Function of Droop Control Considering Dynamic Interaction between Converters

As shown in Fig. 1(a), mathematical expression of $V_{\text{r}k}(s)$ can be written as:

$$V_{\text{r}k}(s) = R_{\text{dsk}}(I_k - I_{\text{Leq}}p_k) = rC_{\text{eq}}sV = k_{\text{r}k}sV \tag{11}$$

where R_{dsk} is virtual resistance of k^{th} LRC, which is defined as r/p_k, r is virtual resistance. Taking droop controller $V_{\text{r}k}(s)$ into account, then voltage closed-loop transfer function $G_{\text{vivrfc}k}(s)$ of k^{th} LRC can be written as:

$$G_{\text{vivrfc}k}(s) = \frac{G_{\text{vd}k}(s)G_{\text{ic}k}(s)G_{\text{vc}k}(s)}{\left\{ \begin{array}{c} \sum_{x=1}^{n}\{G_{\text{vd}x}(s)G_{\text{ic}x}(s)(G_{\text{vc}x}(s)(1+rC_{\text{eq}}s) \\ +p_x G_{\text{iv}}(s))\}+\sum_{x=1}^{n}\{(K_{1x}+K_{2x}s)G_{\text{vd}x}(s)\}+1 \end{array} \right\}} \tag{12}$$

Based on (12), effect of droop controller $V_{\text{r}k}(s)$ on k^{th} LRC can be analyzed. But system-level effect of multiple droop controllers on the system can't be analyzed based on (12). Then, transfer function $G_{\text{vivrsys}}(s)$ of the system can be obtained by adding transfer function $G_{\text{vivrfc}k}(s)$ to each other.

2) Design of Droop Control Parameters Considering Dynamic Interaction between Converters

Transfer function $G_{\text{vivrsys}}(s)$ is system-level result of dynamic interaction between converters, which contains all circuit parameters and control parameters of the MVDC power

system. Except for unknown virtual resistor r, state feedback control, current control and voltage control parameters have been designed. For this purpose, virtual resistor r can be determined from the expected damping factor of dominant poles of transfer function $G_{\mathrm{vivrsys}}(s)$. Then, virtual resistor R_{dsk} of k^{th} LRC will be calculated by (29). So far, all control parameters (including state feedback, current, voltage and droop control parameters) of the system have been designed.

III. Control Parameter Sharing Method

As mentioned above, system-level control parameters design procedure may encounter computational difficulties in an MVDC power system with a large number of converters. Then, a control parameter sharing method between converter and equivalent reduced-order model for designing system dynamic stability is proposed.

A. Sharing Principle of State Feedback Control Parameters

When influence of cable can be ignored in Fig. 1(b), control-to-output transfer function $G_{\mathrm{vdeq}}(s)$ can be written as:

$$G_{\mathrm{vdeq}}(s)=\left(\frac{V_{\mathrm{s}}}{C_{\mathrm{eq}}L_{\mathrm{eq}}}\right)\frac{1}{s^2-\frac{1}{R_{\mathrm{eq}}C_{\mathrm{eq}}}s+\frac{1}{L_{\mathrm{eq}}C_{\mathrm{eq}}}} \tag{13}$$

where V_{s} is input voltage of equivalent reduced-order model. As mentioned above, a state feedback control method is introduced, which can extend stability margin of equivalent reduced-order model, as shown below.

$$f_{\mathrm{ceq}}(s)=(K_{1\mathrm{eq}}+K_{2\mathrm{eq}}s) \tag{14}$$

where $K_{1\mathrm{eq}}$ and $K_{2\mathrm{eq}}$ are proportional and derivative feedback control gains of state feedback control $f_{\mathrm{ceq}}(s)$, respectively. Taking state feedback control $f_{\mathrm{ceq}}(s)$ into account, control-to-inductor current transfer function $G_{\mathrm{idfceq}}(s)$ can be written as:

$$G_{\mathrm{idfceq}}(s)=\frac{\frac{V_{\mathrm{s}}}{L_{\mathrm{eq}}C_{\mathrm{eq}}}G_{\mathrm{iv}}(s)}{s^2+\left(\frac{K_{2\mathrm{eq}}V_{\mathrm{s}}}{L_{\mathrm{eq}}C_{\mathrm{eq}}}-\frac{1}{R_{\mathrm{eq}}C_{\mathrm{eq}}}\right)s+\left(\frac{K_{1\mathrm{eq}}V_{\mathrm{s}}}{L_{\mathrm{eq}}C_{\mathrm{eq}}}+\frac{1}{L_{\mathrm{eq}}C_{\mathrm{eq}}}\right)} \tag{15}$$

In order to get desired dynamic characteristics, $K_{1\mathrm{eq}}$ and $K_{2\mathrm{eq}}$ can be turned according to given natural angular frequency ω_{feq} and damping factor ζ_{feq}, according to formulas as follows:

$$\begin{cases} K_{1\mathrm{eq}}=\left(\omega_{\mathrm{feq}}^2+\dfrac{1}{L_{\mathrm{eq}}C_{\mathrm{eq}}}\right) \\ K_{2\mathrm{eq}}=\left(2\zeta_{\mathrm{feq}}\omega_{\mathrm{feq}}+\dfrac{1}{R_{\mathrm{eq}}C_{\mathrm{eq}}}\right) \end{cases} \tag{16}$$

In order to ensure expected dynamic stability of system, state feedback control parameters $K_{1\mathrm{eq}}$ and $K_{2\mathrm{eq}}$ designed based on equivalent reduced-order model should be shared with each LRC. Moreover, sharing principle of state feedback control parameters $K_{1\mathrm{eq}}$ and $K_{2\mathrm{eq}}$ should be based on dynamic characteristics of each LRC, as shown in (17).

$$\begin{cases} K_{1k}=K_{1\mathrm{eq}} \\ K_{2k}=K_{2\mathrm{eq}} \end{cases} \tag{17}$$

As expected, K_{1k} is equal to $K_{1\mathrm{eq}}$, and K_{2k} is also consistent with $K_{2\mathrm{eq}}$. With transfer functions shown in (17), sharing principle of state feedback control parameters between k^{th} LRC and equivalent reduced-order model are established.

B. Sharing Principle of Current Control Parameters

As shown in Fig. 1(b), current controller of equivalent reduced-order model can be written as:

$$G_{\mathrm{iceq}}(s)=k_{\mathrm{pieq}}+\frac{k_{\mathrm{iieq}}}{s}=k_{\mathrm{pieq}}\left(1+\frac{\omega_{\mathrm{iLeq}}}{s}\right) \tag{18}$$

where k_{pieq} and k_{iieq} are proportional and integral gains of current controller $G_{\mathrm{iceq}}(s)$, respectively. As given in (19), an inverted zero is added to current control loop of equivalent reduced-order model, at frequency f_{iLeq}.

Loop gain $T_{\mathrm{iifceq}}(s)$ and closed-loop transfer function $G_{\mathrm{iifceq}}(s)$ of current control of equivalent reduced-order model can be obtained, as shown in (19) and (20), respectively.

$$T_{\mathrm{iifceq}}(s)=G_{\mathrm{idfceq}}(s)G_{\mathrm{iceq}}(s) \tag{19}$$

$$G_{\mathrm{iifceq}}(s)=\frac{G_{\mathrm{vdeq}}(s)G_{\mathrm{iceq}}(s)G_{\mathrm{iv}}(s)}{\left\{\begin{array}{c}1+G_{\mathrm{vdeq}}(s)(K_{1\mathrm{eq}}+K_{2\mathrm{eq}}s)\\ +G_{\mathrm{vdeq}}(s)G_{\mathrm{iceq}}(s)G_{\mathrm{iv}}(s)\end{array}\right\}} \tag{20}$$

It is assumed ω_{iceq} is crossover frequency of current control loop of equivalent reduced-order model, and η_{ieq} is defined as ratio of ω_{iLeq} to ω_{iceq}.

In this paper, ratio of crossover frequency ω_{iceq} to switching frequency of equivalent reduced-order model is chosen to be 0.1. In order to avoid changing crossover frequency ω_{iceq}, magnitude of loop gain $T_{\mathrm{iifceq}}(s)$ should be united at crossover frequency ω_{iceq}. This usually requires η_{ieq} be selected as 0.1. In addition, other values of η_{ieq} can be selected when a pole needs to be cancelled by zero generated by current controller $G_{\mathrm{iceq}}(s)$. For example, with increase of η_{ieq}, zero generated by current controller $G_{\mathrm{iceq}}(s)$ will move to the left in s plane.

Sharing principle of current control parameters should be based on dynamic characteristics of each LRC, as shown in (21).

$$\begin{cases} k_{\mathrm{pi}k}=\dfrac{k_{\mathrm{pieq}}L_{\mathrm{f}k}}{L_{\mathrm{eq}}} \\ k_{\mathrm{ii}k}=\dfrac{k_{\mathrm{iieq}}L_{\mathrm{f}k}}{L_{\mathrm{eq}}} \end{cases} \tag{21}$$

As it was expected, $k_{\mathrm{pi}k}$ is a function of k_{pieq}, $L_{\mathrm{f}k}$ and L_{eq}, while $k_{\mathrm{ii}k}$ is a function of k_{iieq}, $L_{\mathrm{f}k}$ and L_{eq}. With transfer functions shown in (21), sharing principle of current control parameters between k^{th} LRC and equivalent reduced-order model are established.

C. Sharing Principle of Voltage Control Parameters

As shown in Fig. 1(b), voltage controller of equivalent reduced-order model can be written as

$$G_{\mathrm{ivdfceq}}(s)=\frac{G_{\mathrm{iifceq}}(s)}{G_{\mathrm{iv}}(s)} \tag{22}$$

$$G_{\mathrm{vceq}}(s)=k_{\mathrm{pveq}}+\frac{k_{\mathrm{iveq}}}{s}=k_{\mathrm{pveq}}\left(1+\frac{\omega_{\mathrm{vLeq}}}{s}\right) \tag{23}$$

where k_{pveq} and k_{iveq} are proportional and integral gains of voltage controller $G_{\mathrm{vceq}}(s)$. As given in (23), an inverted zero

is added to voltage control loop of equivalent reduced-order model, at frequency f_{vLeq}.

Loop gain $T_{\mathrm{vivfceq}}(s)$ and closed-loop transfer function $G_{\mathrm{vivfceq}}(s)$ of voltage control of equivalent reduced-order model can be obtained, as shown in (24) and (25), respectively.

$$T_{\mathrm{vivfceq}}(s) = G_{\mathrm{ivdfceq}}(s)G_{\mathrm{vceq}}(s) \tag{24}$$

$$G_{\mathrm{vivfceq}}(s) = \frac{G_{\mathrm{vdeq}}(s)G_{\mathrm{iceq}}(s)G_{\mathrm{vceq}}(s)}{\left\{\begin{array}{c} G_{\mathrm{vdeq}}(s)G_{\mathrm{iceq}}(s)\{G_{\mathrm{vceq}}(s)+G_{\mathrm{iv}}(s)\} \\ +G_{\mathrm{vdeq}}(s)(K_{1\mathrm{eq}}+K_{2\mathrm{eq}}s)+1 \end{array}\right\}} \tag{25}$$

It is assumed ω_{vceq} is crossover frequency of voltage control loop of equivalent reduced-order model, and η_{veq} is defined as ratio of ω_{vLeq} to ω_{vceq}.

In this paper, ratio of ω_{vceq} to ω_{iceq} is chosen to be between 0.1 and 0.5. In order to avoid changing crossover frequency ω_{vceq}, magnitude of loop gain $T_{\mathrm{vivfceq}}(s)$ should be united at crossover frequency ω_{vceq}. This usually requires η_{veq} should be selected as 0.1. In addition, other values of η_{veq} can be selected when a pole needs to be cancelled by zero generated by voltage controller $G_{\mathrm{vceq}}(s)$. For example, with increase of η_{veq}, zero generated by voltage controller $G_{\mathrm{vceq}}(s)$ will move to the left in s plane.

Sharing principle of voltage control parameters should be based on dynamic characteristics of each LRC, as shown in (26).

$$\left\{\begin{array}{l} k_{\mathrm{pv}k} = \left(\dfrac{k_{\mathrm{pieq}}}{L_{\mathrm{eq}}}\right)\left(\dfrac{k_{\mathrm{pveq}}L_{\mathrm{f}k}p_k}{k_{\mathrm{pi}k}}\right) \\ k_{\mathrm{iv}k} = \left(\dfrac{k_{\mathrm{iieq}}}{L_{\mathrm{eq}}}\right)\left(\dfrac{k_{\mathrm{iveq}}L_{\mathrm{f}k}p_k}{k_{\mathrm{ii}k}}\right) \end{array}\right. \tag{26}$$

As it was expected, $k_{\mathrm{pv}k}$ is a function of k_{pieq}, L_{eq}, k_{pveq}, $L_{\mathrm{f}k}$, $k_{\mathrm{pi}k}$ and p_k, while $k_{\mathrm{iv}k}$ is a function of k_{iieq}, L_{eq}, k_{iveq}, $L_{\mathrm{f}k}$, $k_{\mathrm{ii}k}$ and p_k. With transfer functions shown in (26), sharing principle of voltage control parameters between k^{th} LRC and equivalent reduced-order model are established.

D. Sharing Principle of Droop Control Parameters

As shown in Fig. 1(b), droop controller of equivalent reduced-order model can be written as:

$$V_{\mathrm{refd}}(s) = r(I_{\mathrm{Leq}} - I) = (rC_{\mathrm{eq}}V)s \tag{27}$$

Taking droop controller $V_{\mathrm{refd}}(s)$ into account, voltage closed-loop transfer function $G_{\mathrm{vivrfc}}(s)$ can be written as (28).

$$G_{\mathrm{vivrfceq}}(s) = \frac{G_{\mathrm{vdeq}}(s)G_{\mathrm{iceq}}(s)G_{\mathrm{vceq}}(s)}{\left\{\begin{array}{c} G_{\mathrm{vdeq}}(s)G_{\mathrm{iceq}}(s)\{G_{\mathrm{vceq}}(s)(1+rC_{\mathrm{eq}}s)+G_{\mathrm{iv}}(s)\} \\ +G_{\mathrm{vdeq}}(s)(K_{1\mathrm{eq}}+K_{2\mathrm{eq}}s)+1 \end{array}\right\}} \tag{28}$$

Virtual resistance r can be determined to accomplish expected damping factor. Sharing principle of droop control parameters between k^{th} LRC and VESGM is (29).

$$R_{\mathrm{ds}k} = \frac{r}{p_k} \tag{29}$$

IV. Theoretical Analysis and Experimental Verification

In order to verify validity of system-level control parameters design procedure and control parameters sharing method, two multi-converters MVDC power systems (system I and system II) are implemented in a RT-BOX hardware-in-the-loop experimental platform shown in Fig. 3. Topologies of tested system I and system II are shown in Figs. 4 and 5, respectively.

Main circuit parameters of the system I and system II are shown in Tables II and III, respectively.

Control parameters of system I for case 1 to case 5 are shown in Table IV. In addition, control parameters under case

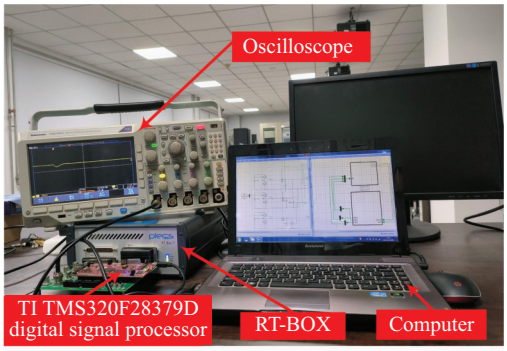

Fig. 3. RT-BOX hardware-in-the-loop experimental platform.

TABLE II
Parameters of System I

	Parameter	Value
1^{th} LRC	Rated output power P_{n1} (MW)	5
	Filter inductor L_{f1} (mH)	26.67
	Filter capacitor C_{f1} (mF)	0.0937
	Switching frequency f_{s1} (kHz)	1
2^{th} LRC	Rated output power P_{n2} (MW)	5
	Filter inductor L_{f2} (mH)	26.67
	Filter capacitor C_{f2} (mF)	0.0937
	Switching frequency f_{s2} (kHz)	1
CPL	Rated output power P_{eq} (MW)	2
	Input filter capacitor C_{Leq} (mF)	0.2
	Number	5
Cable	Cable inductor (mH/km)	0.47
	Cable capacitor (mΩ/km)	22.1
	Length (km)	2
	Number	5

TABLE III
Parameters of System II

	Parameter	Value
1^{th} LRC	Rated output power P_{n1} (MW)	2
	Filter inductor L_{f1} (mH)	66.7
	Filter capacitor C_{f1} (mF)	0.0375
	Switching frequency f_{s1} (kHz)	1
2^{th} LRC	Rated output power P_{n2} (MW)	8
	Filter inductor L_{f2} (mH)	16.67
	Filter capacitor C_{f2} (mF)	0.15
	Switching frequency f_{s2} (kHz)	1
CPL	Rated output power P_{eq} (MW)	2
	Input filter capacitor C_{Leq} (mF)	0.2
	Number	5
Cable	Cable inductor (mH/km)	0.47
	Cable capacitor (mΩ/km)	22.1
	Length (km)	2
	Number	5

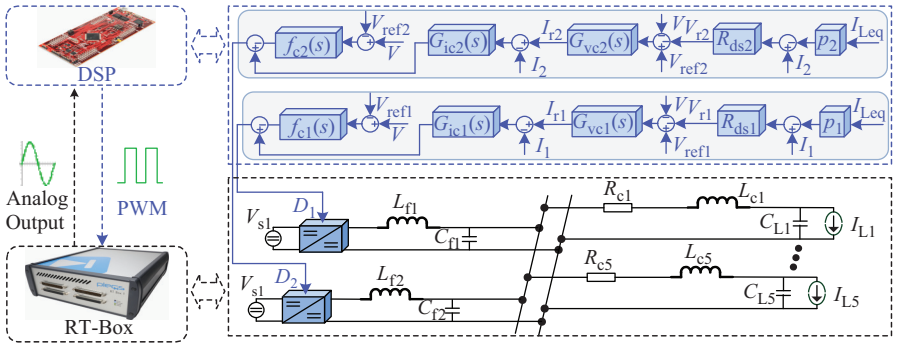

Fig. 4. Topology of the tested system I.

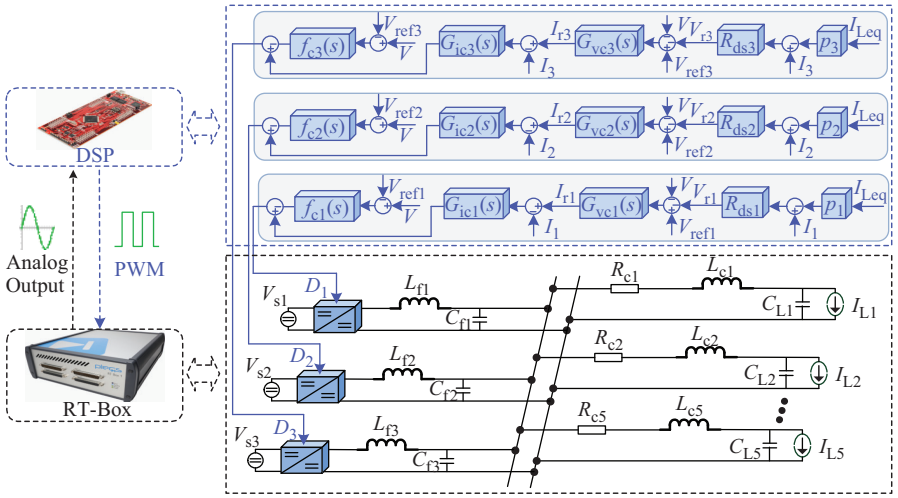

Fig. 5. Topology of the tested system II.

TABLE IV
CONTROL PARAMETERS OF SYSTEM I UNDER CASE 1 TO CASE 5

	Case 1	Case 2	Case 3	Case 4	Case 5
K_{11}	0	0	−59210	−47366	−47366
K_{21}	0	0	172.18	260.14	260.14
k_{pi1}	0.0002	0.0023	0.0027	0.0027	0.0027
k_{ii1}	0.0005	0.1420	0.1670	0.1670	0.1670
k_{pv1}	0.2783	0.0957	0.0661	0.1549	0.3196
k_{iv1}	30.599	50.092	4.1516	29.197	120.49
R_{ds1}	0.1400	0.0800	0.0800	0.0800	0.0800
K_{12}	0	0	−59210	−47366	−47366
K_{22}	0	0	172.18	260.14	260.14
k_{pi2}	0.0002	0.0023	0.0027	0.0027	0.0027
k_{ii2}	0.0005	0.1420	0.1670	0.1670	0.1670
k_{pv2}	0.2783	0.0957	0.0661	0.1549	0.3196
k_{iv2}	30.599	50.092	4.1516	29.197	120.49
R_{ds2}	0.1400	0.0800	0.0800	0.0800	0.0800

TABLE V
CONTROL PARAMETERS FROM CASE 6 TO CASE 9

	System I				System II	
	Case 6	Case 7	Case 8	Case 9	Case 6	Case 7
K_{11}	−47366	−47366	0	0	−47366	−47366
K_{21}	260.14	260.14	0	0	260.14	260.14
k_{pi1}	0.0013	0.0013	0.0023	0.0023	0.0033	0.0033
k_{ii1}	0.0835	0.0835	0.1420	0.1420	0.2087	0.2087
k_{pv1}	0.1085	0.2056	0.0957	0.0957	0.0434	0.0822
k_{iv1}	13.640	51.674	50.092	50.092	5.4561	20.670
R_{ds1}	0.0800	0.0800	0.0800	0.0800	0.2000	0.2000
K_{12}	−47366	−47366	0	0	−47366	−47366
K_{22}	260.14	260.14	0	0	260.14	260.14
k_{pi2}	0.0013	0.0013	0.0023	0.0023	0.0008	0.0008
k_{ii2}	0.0835	0.0835	0.1420	0.1420	0.0522	0.0522
k_{pv2}	0.1085	0.2056	0.0957	0.0957	0.1737	0.3290
k_{iv2}	13.640	51.674	50.092	7.5139	21.824	82.679
R_{ds2}	0.0800	0.0800	0.0800	0.0800	0.0500	0.0500

6 to case 9 are shown in Table V. Corresponding purposes for cases 1 to 9 will be described in detail in subsequent subsections, respectively.

A. Stable Oscillation Frequency Design

In case 1, control parameters of single-converter are designed by control parameter design procedure in [10]. As shown in Fig. 6, log-phase curves of transfer function $G_{\mathrm{viv}}(s)$ have positive phase margin, which means single-converter is stable. Above conclusion can also be verified by zero-pole diagram shown in Fig. 7(a): zeros and poles of single-converter are all listed in the left-half s plane.

However, when two converters in the system I adopt control parameters of above single-converter situation, there is a stability problem. As shown in Fig. 7(b), system I has a pair of conjugate poles which are listed in the right-half s plane, which means system I is unstable. The above conclusion can also be verified by bode diagram shown in Fig. 6: log-phase curves of transfer functions $G_{\mathrm{viv1}}(s)$ has a negative phase margin.

In case 2, values of $\omega_{\mathrm{ic}k}$, η_{ik}, $\omega_{\mathrm{vc}k}$ and $\eta_{\mathrm{v}k}$ are consistent

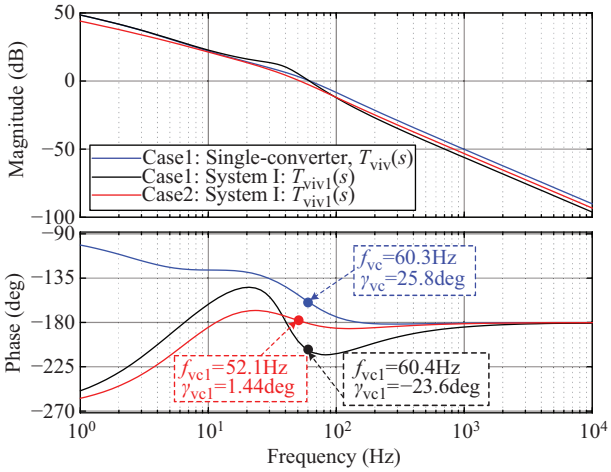

Fig. 6. Bode diagram of case 1 and case 2.

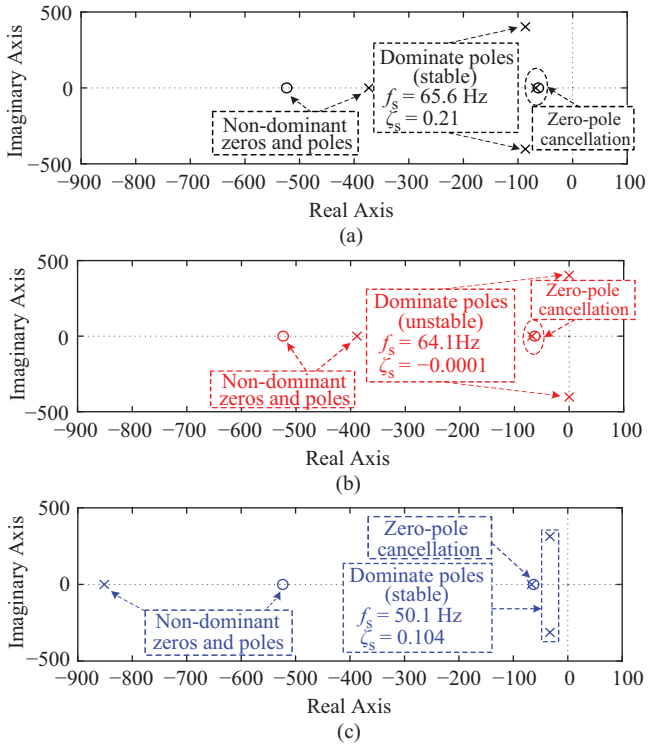

Fig. 7. Zero-pole diagram. (a) single-converter of case 1. (b) System I of case 1. (c) System I of case 2.

with those in the above first step of individual control parameters design procedure ($k = 1, 2$). As shown in Fig. 6, log-phase curves of transfer function $G_{\mathrm{viv1}}(s)$ has positive phase margin, which means 1^{th} LRC in system I is stable. Furthermore, conclusion system I under case 2 is stable can be obtained by zero-pole diagram: zeros and poles are all listed in the left-half s plane shown in Fig. 7(c). In addition, due to zero-pole cancellation, system I under case 2 can be approximated by a second-order model. Then, oscillation frequency and damping factor of system can be calculated based on dominant conjugate poles.

Comparing case 1 and case 2, effectiveness of system-level control parameters design procedure is verified in this section. Additionally, origin of effectiveness should be figured out. For instance, control-to-inductor current transfer functions used by the two design procedures are very different: transfer function $G_{\mathrm{id}}(s)$ has positive phase margin, while transfer function $G_{\mathrm{id1}}(s)$ has a negative phase margin, as shown in Fig. 6.

Experimental verifications have been provided, as shown in Fig. 8. In case 1, DC bus voltage of single-converter situation can be stabilized after a short transient process when power of resistive load changes from 1.875 MW to 3.625 MW. Moreover, stable oscillation frequency of single-converter situation in Fig. 8 is about 68.05 Hz, which is basically consistent with theoretical value of 65.6 Hz in Fig. 7(a). System I under case 1 is unstable after constant power load changes from 2.5 MW to 5 MW. In addition, unstable oscillation frequency of system I under case 1 in Fig. 8 is about 71.74 Hz, which is basically consistent with theoretical value of 67.4 Hz in Fig. 7(b). At the same CPL disturbance, DC bus voltage of system I under case 2 can be stabilized after a short transient process. Stable oscillation frequency of system I under case 2 in Fig. 8 is about 49.0 Hz, which is basically consistent with theoretical value of 50.1 Hz in Fig. 7(c).

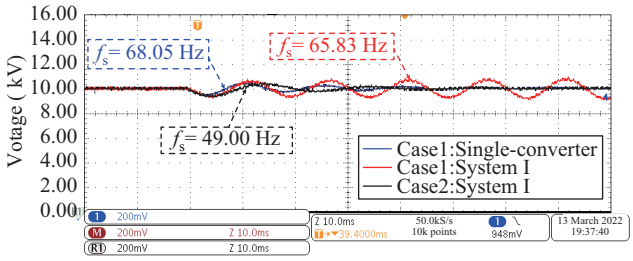

Fig. 8. Experimental waveforms of DC bus voltage under case 1 and case 2.

B. Wide Range Design Capability of Oscillation Frequency

In this section, wide range design capability of system-level control parameters design procedure for oscillation frequency will be introduced in detail. Then, three cases (case 3, case 4 and case 5) with different oscillation frequency design proposes are set. In the above three cases, selected values of $\omega_{\mathrm{ic}k}$, $\eta_{\mathrm{i}k}$ and $\eta_{\mathrm{v}k}$ are $100 * 2 * \pi$, 0.1 and 1, respectively. For $\omega_{\mathrm{vc}k}$, selected values for case 3, case 4 and case 5 are $10{*}2{*}\pi$, $30 * 2 * \pi$ and $60 * 2 * \pi$, respectively.

As shown in Fig. 9, increasing crossover frequency $\omega_{\mathrm{vc}k}$, crossover frequency of $T_{\mathrm{vivfc}k}(s)$ will be increased with positive phase margin. According to frequency domain curves of transfer function $G_{\mathrm{vivrfc}k}(s)$ depicted in Fig. 10, control bandwidths $\omega_{\mathrm{vb}k}$ of case 3, case 4 and case 5 are known to be $18.6 * 2 * \pi$ rad/s, $41 * 2 * \pi$ rad/s and $86.7 * 2 * \pi$ rad/s, respectively. This means oscillation frequency of system I will be increased with positive damping factor, as shown in Fig. 11. In addition, due to zero-pole cancellation, system I under above three cases can be approximated by a second-order model, respectively. Then, oscillation frequency and damping factor of system can be calculated based on dominant conjugate poles.

Experimental verifications have been provided, as shown in Fig. 12. Corresponding results of case 3, case 4 and case 5 represent significantly uniform oscillation frequency in

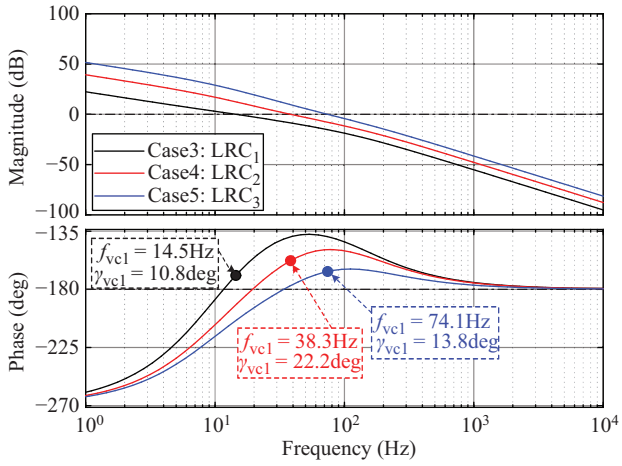

Fig. 9. Bode diagram of $T_{\mathrm{vivfc}k}(s)$ under case 3, case 4, and case 5.

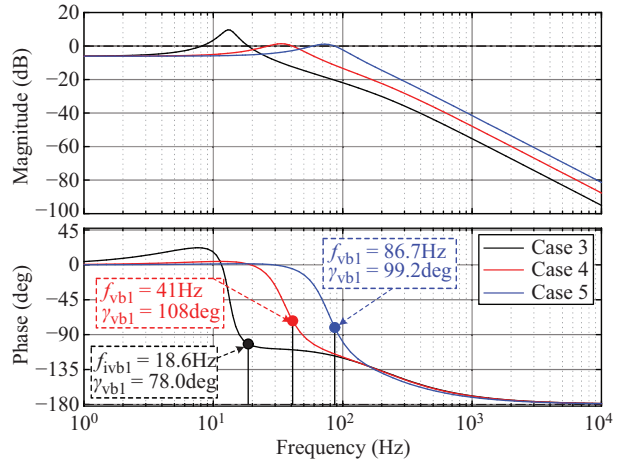

Fig. 10. Bode diagram of $G_{\mathrm{vivrfc}k}(s)$ under case 3, case 4, and case 5.

accordance with Fig. 11. Consequently, oscillation frequency of DC bus voltage in a wide oscillation frequency range (such as 10–70 Hz) can be designed accurately.

C. Consistent Dynamic Characteristic Design of Different Systems

Dynamic stability of system can be guaranteed based on system-level control parameters design procedure, but calculation burden of control parameters is too heavy. Then, effectiveness of the sharing principle of control parameters designed by equivalent reduced-order model (EROM) will be introduced, as detailed in case 6 and case 7. For system I and system II, filter parameters of their equivalent reduced-order model are the same. Therefore, based on control parameters design of same equivalent reduced-order model, consistent dynamic characteristic design of different systems can be realized in this paper.

As shown in Fig. 13, theoretical crossover frequency of $T_{\mathrm{vivfc}}(s)$ increase which is the result of increased preset crossover frequency ω_{vc}. This means oscillation frequency of equivalent reduced-order model will be increased with increased crossover frequency ω_{vc}, which can be verified by zero-pole diagram shown in Fig. 14 intuitively. According to

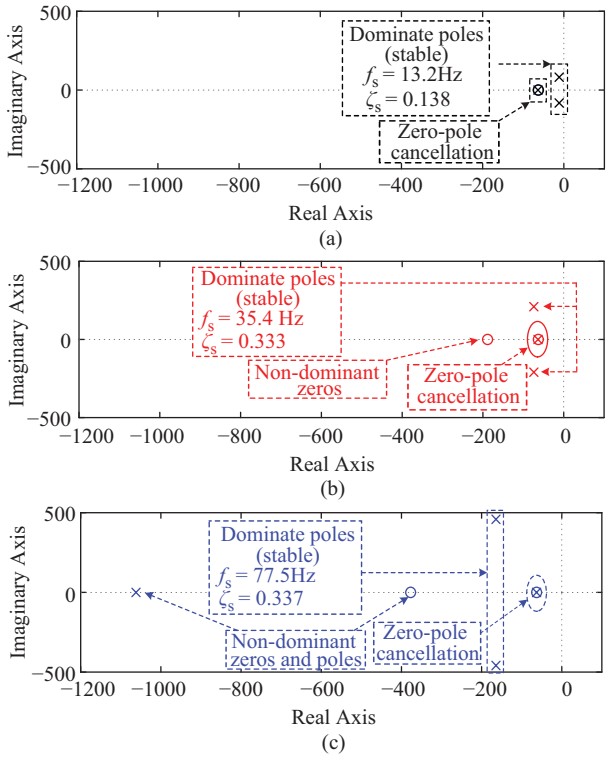

Fig. 11. Zero-pole diagram under case 3, case 4 and case 5. (a) System I of case 3. (b) System I of case 4. (c) System I of case 5.

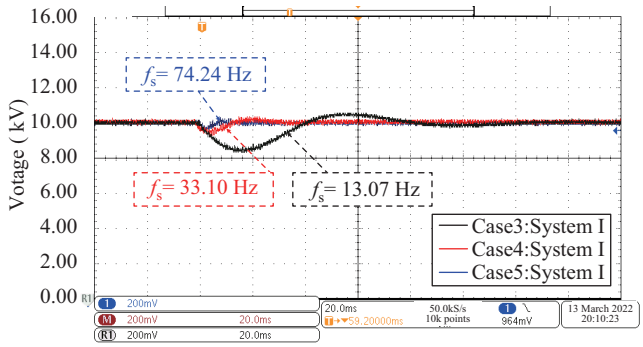

Fig. 12. Experimental waveforms of DC bus voltage under case 3, case 4 and case 5.

Fig. 14, equivalent reduced-order model can be approximated by a second-order model. Then, oscillation frequency and damping factor of system can be calculated based on dominant conjugate poles.

Based on the proposed control parameters sharing method, control parameters of each converter in the system can be obtained quantitatively. Since parameters of each LRC in system I are consistent, and voltage-current closed-loop transfer function of equivalent reduced-order model and k^{th} LRC can be obtained, as shown in (30), (31) and (32) respectively. For system I, zeros and poles of each transfer function $G_{\mathrm{vivrfc}k}(s)$ are consistent with transfer function $G_{\mathrm{vivrfceq}}(s)$. In addition, transfer function $G_{\mathrm{vivrfceq}}(s)$ can be obtained by adding transfer function $G_{\mathrm{vivrfc}k}(s)$ to each other. The above conclusion can also be verified by bode diagram and unit step response shown in Figs. 15 and 16 respectively. For system

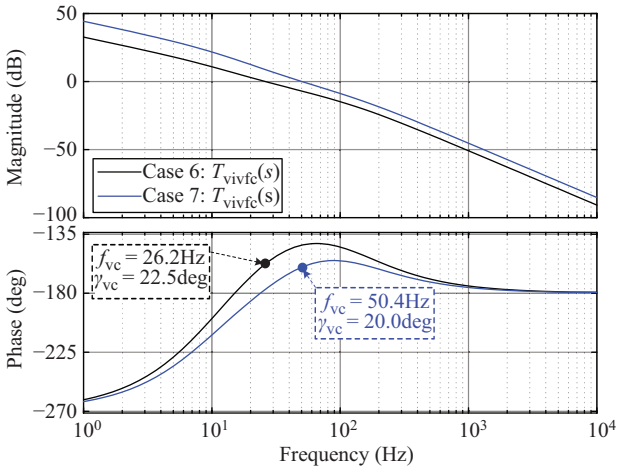

Fig. 13. Bode diagram of case 6 and case 7.

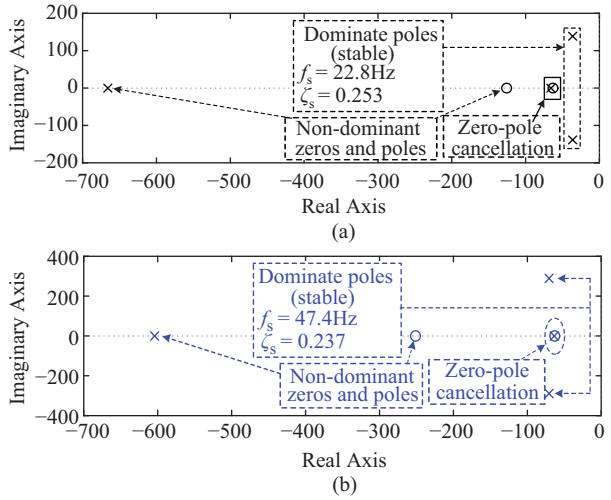

Fig. 14. Zero-pole diagram. (a) Case 6. (b) Case 7.

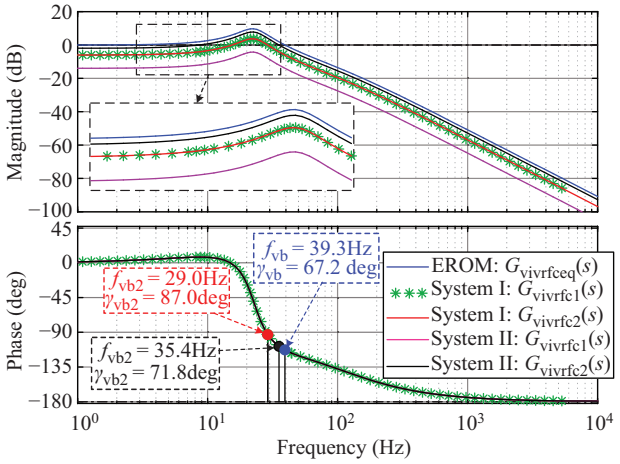

Fig. 15. Bode diagram of case 6.

II, zeros and poles of each transfer function $G_{\mathrm{vivrfc}k}(s)$ are also consistent with transfer function $G_{\mathrm{vivrfceq}}(s)$, as shown in (30), (33) and (34) respectively. In system II, transfer function $G_{\mathrm{vivrfceq}}(s)$ can also be obtained by adding transfer

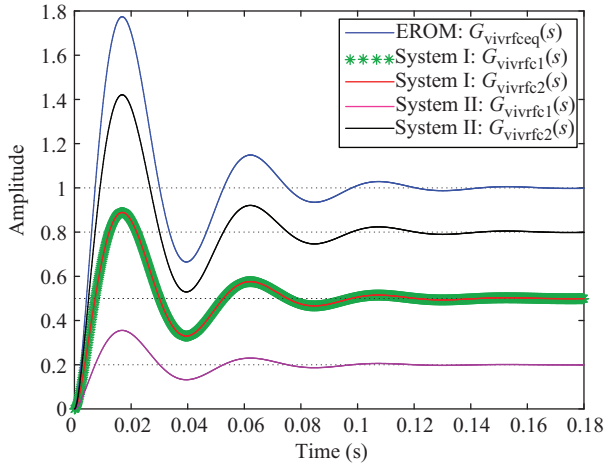

Fig. 16. Unit step response of case 6.

function $G_{\mathrm{vivrfc}k}(s)$ to each other, as shown in Figs. 15 and 16 respectively. In system I, control bandwidth $\omega_{\mathrm{vb}k}$ of voltage closed-loop transfer function for both LRCs is $29*2*\pi$ rad/s. For system II, control bandwidth ω_{vb2} of voltage closed-loop transfer function of the 2^{th} LRC can be identified as $35.4*2*\pi$ rad/s.

$$G_{\mathrm{vivrfceq}}(s) = \frac{(2.1565\times10^5)(s+251.3)(s+62.83)}{(s+604.1)(s+63.59)(s^2+141.2s+8.865\times10^4)} \tag{30}$$

$$G_{\mathrm{vivrfc1}}(s) = \frac{(1.0782\times10^5)(s+251.3)(s+62.83)}{(s+604.1)(s+63.59)(s^2+141.2s+8.865\times10^4)} \tag{31}$$

$$G_{\mathrm{vivrfc2}}(s) = \frac{(1.0782\times10^5)(s+251.3)(s+62.83)}{(s+604.1)(s+63.59)(s^2+141.2s+8.865\times10^4)} \tag{32}$$

$$G_{\mathrm{vivrfc1}}(s) = \frac{(43130)(s+251.3)(s+62.83)}{(s+604.1)(s+63.59)(s^2+141.2s+8.865\times10^4)} \tag{33}$$

$$G_{\mathrm{vivrfc2}}(s) = \frac{(1.7252\times10^5)(s+251.3)(s+62.83)}{(s+604.1)(s+63.59)(s^2+141.2s+8.865\times10^4)} \tag{34}$$

In order to verify effectiveness of the proposed control parameters sharing method, bode diagram and unit step response diagram of case 7 are also given, as shown in Figs. 17 and 18, respectively.

Corresponding experimental results of case 6 and case 7, which are plotted in Fig. 19, represent significantly uniform steady-state and dynamic-state performance of DC bus voltage among system I, system II and their consistent equivalent reduced-order model. In addition, corresponding results of case 6 and case 7 represent significantly uniform oscillation frequency in accordance with Fig. 14. The fundamental reason

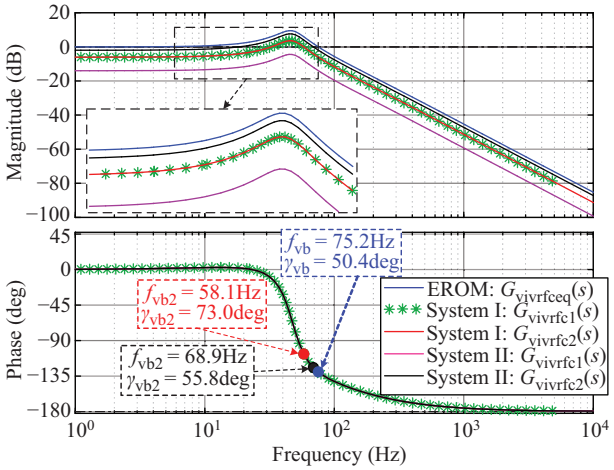

Fig. 17. Bode diagram of case 7.

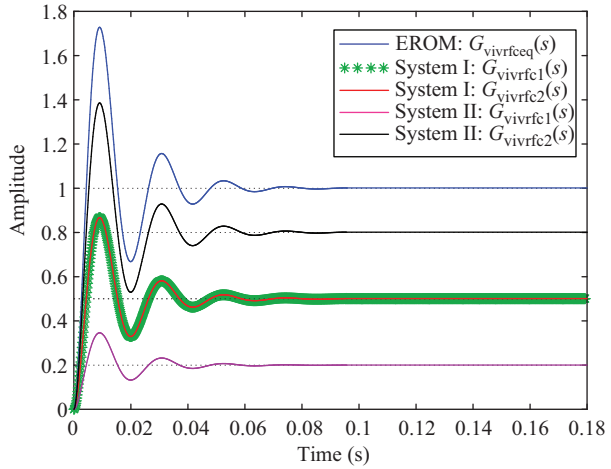

Fig. 18. Unit step response of case 7.

for the above results is application of control parameters sharing method proposed in this paper.

Consequently, correctness of control parameter sharing method is verified, even if parameters of converters in system are different. This means control parameters of multi-converters MVDC power system can be designed by its equivalent reduced-order model.

D. Dynamic Interaction Analysis

Due to dynamic interaction between converters in a DC system, change of control parameters of one converter will inevitably affect dynamic behavior of other converters. Then, two cases with different design proposes are set, as shown in case 8 and case 9. In case 8, values of $\omega_{\mathrm{ic}k}$, $\eta_{\mathrm{i}k}$, $\omega_{\mathrm{vc}k}$ and $\eta_{\mathrm{v}k}$ are consistent with those in single-converter situation ($k = 1$, 2). While in case 9, value of $\eta_{\mathrm{v}2}$ is selected as 1.25, and other parameters are consistent with case 8.

As shown in Fig. 20, log-phase curves of transfer function $T_{\mathrm{viv1}}(s)$ under case 8 have positive phase margin. This means the damping factor is positive, which can be verified by zero-pole diagram shown in Fig. 22 intuitively. According to Fig. 22, system I under case 8 can be approximated by a second-order system. Then, oscillation frequency and damping factor of system can be calculated based on dominant conjugate poles.

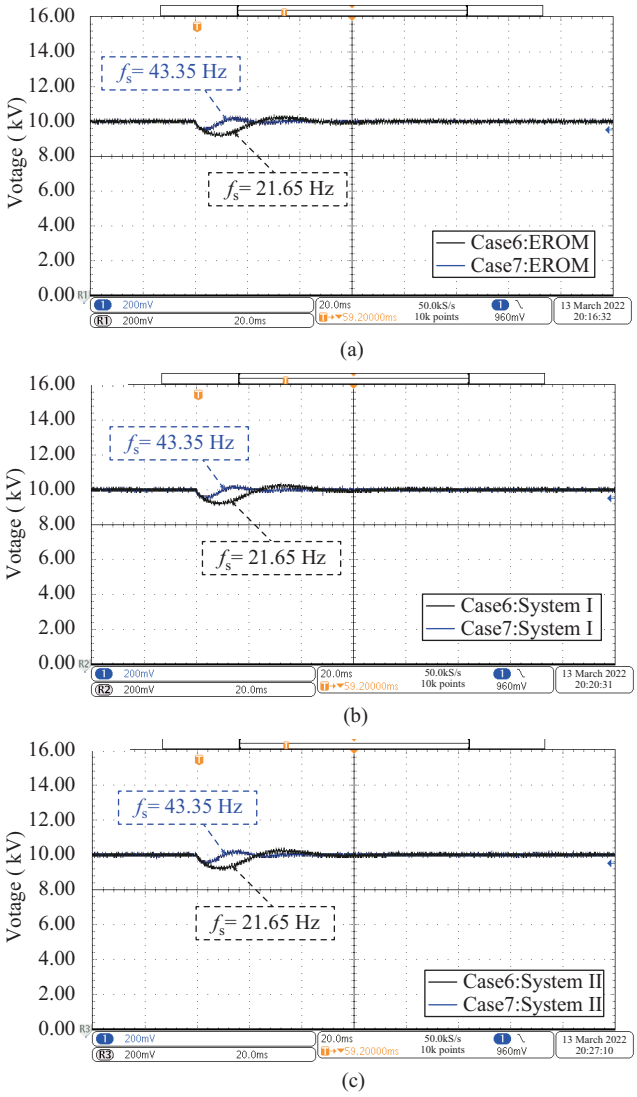

Fig. 19. Experimental waveforms of DC bus voltage. (a) Equivalent reduced-order model. (b) System I. (c) System II.

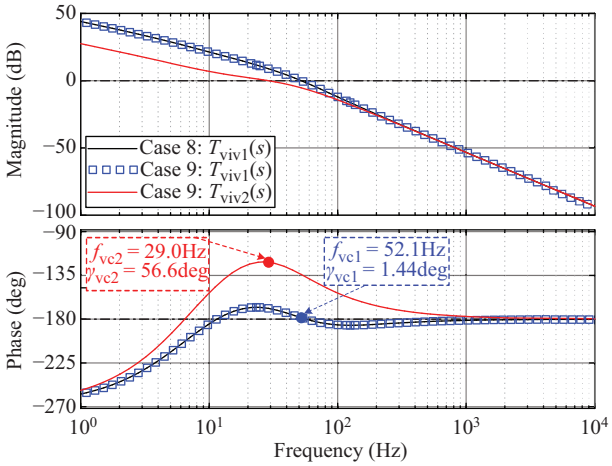

Fig. 20. Bode diagram of $T_{\mathrm{vivk}}(s)$ under case 8 and case 9.

Compared with case 8, crossover frequency f_{vc2} of transfer function $T_{\mathrm{viv2}}(s)$ decrease with decrease of η_{v2}, as shown in Fig. 21. Due to dynamic interaction between converters, control bandwidth f_{vb1} of transfer function $G_{\mathrm{vivr1}}(s)$ will also be reduced as shown in Fig. 21. Then oscillation frequency of system will be reduced with increased damping, which can be verified by zero-pole diagram shown in Fig. 22 intuitively.

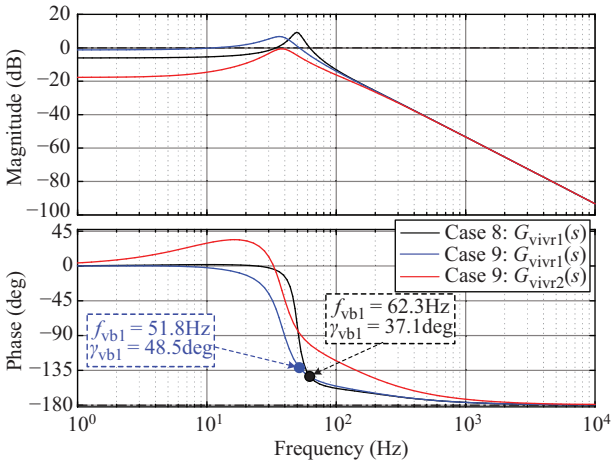

Fig. 21. Bode diagram of $G_{\mathrm{vivfck}}(s)$ under case 8 and case 9.

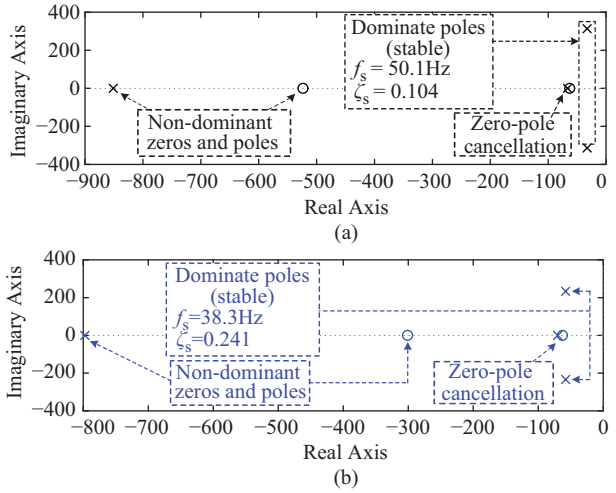

Fig. 22. Zero-pole diagram. (a) Case 8. (b) Case 9.

Experimental verifications have been provided, as shown in Figs. 23 and 24. Corresponding results, which are plotted in Fig. 23, represent significantly uniform oscillation frequency and damping factor in accordance with Fig. 22. As shown in Fig. 24, current overshoot of LRC_1 is larger than LRC_2, which verified theoretical design goal that response speed of LRC_1 is faster than LRC_2 under case 9. Consequently, correctness of the proposed system-level control parameters design procedure is verified, even if dynamic characteristics of each converter are different.

V. Conclusion

Open-loop and closed-loop transfer functions of each control loop of converter are established in this paper, which

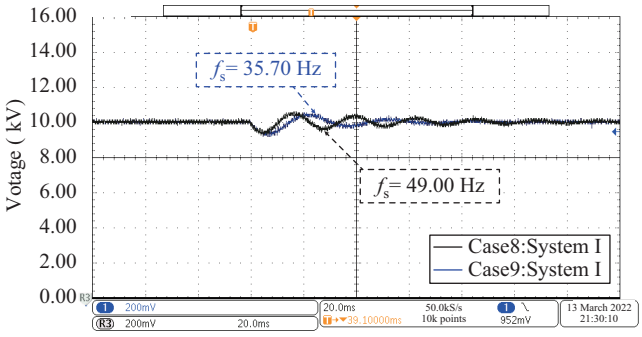

Fig. 23. Experimental waveforms under case 8 and case 9.

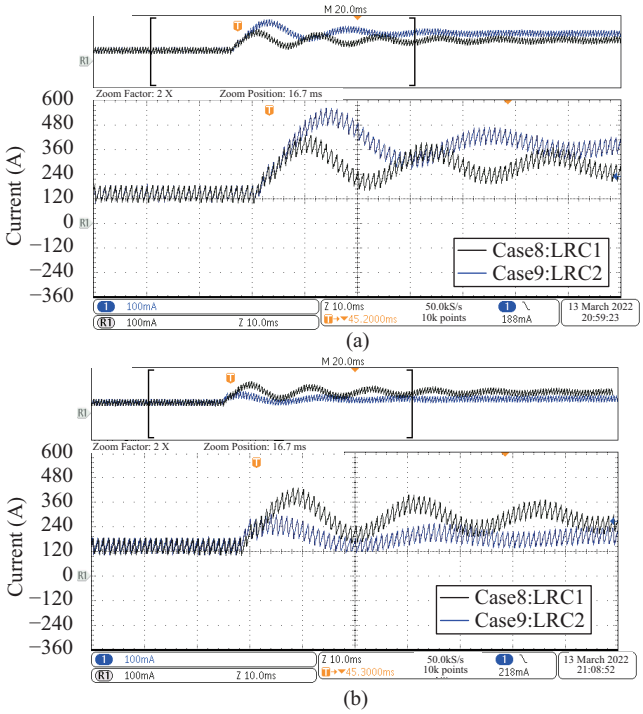

Fig. 24. Experimental waveforms. (a) LRC_1. (b) LRC_2.

considers dynamic interaction between converters in multi-converters MVDC power system. Moreover, number of poles (or zeros) of transfer function considering dynamic interaction between converters is very consistent with single-converter situation. This means, with the above transfer functions, control parameters design complexity of system can be reduced significantly. In addition, dynamic interaction mechanism voltage control dynamics of a converter affected by other converters can be evaluated based on voltage closed-loop transfer function accurately.

System-level control parameters design procedure proves to be an effective tool for simplifying control parameters design of multi-converters MVDC power system. In this design procedure, control parameters of all converters are designed from the point of view of system dynamic stability. Through mutual cancellation of some zeros and poles, system can be designed as a second-order model. Then, oscillation frequency and damping factor of system can be evaluated accurately. In addition, control objectives of each converter with different

dynamic characteristics can be achieved, which depends on selection of different design principles.

Based on dynamic interaction mechanism between converters of each control loop in the system, a control parameter sharing method is proposed. With this sharing method, control parameters of equivalent reduced-order model of system are shared with each converter. Then, oscillation frequency and damping factor of DC bus voltage in a wide oscillation frequency range (such as 10–70 Hz) can be designed accurately.

For stability problems of multi-converters MVDC power systems caused by loss of source converters, controller output limit, duty saturation, topology change, inaccurate circuit parameters, etc., corresponding control parameter redesign methods will be discussed in depth subsequently.

APPENDIX

A. Detailed Deduction of Current Control Transfer Function

As can be seen from Fig. 1, multi-converters MVDC power system can be established as:

$$V=\sum_{x=1}^{n}\{G_{\mathrm{vd}x}(s)D_x(s)\} \tag{A1}$$

Taking state feedback control and current control into account, duty $D_k(s)$ of k^{th} LRC can be obtained, as shown in (A2).

$$D_k(s)=G_{\mathrm{ic}k}(s)(I_{\mathrm{r}k}-I_k)-f_{ck}(s)V \tag{A2}$$

Combining (A2) to (A1), multi-converters MVDC power system can be written as:

$$\begin{aligned}V=&\sum_{x=1}^{n}\{G_{\mathrm{vd}x}(s)G_{\mathrm{ic}x}(s)(I_{\mathrm{r}x}-I_x)\}\\&-\sum_{x=1}^{n}\{G_{\mathrm{vd}x}(s)f_{cx}(s)V\}\end{aligned} \tag{A3}$$

It can represent (A3) as (A4):

$$\begin{aligned}&\left\{1+\sum_{x=1}^{n}(G_{\mathrm{vd}x}(s)f_{cx}(s))\right\}V\\&=\sum_{x=1}^{n}\{G_{\mathrm{vd}x}(s)G_{\mathrm{ic}x}(s)(I_{\mathrm{r}x}-I_x)\}\end{aligned} \tag{A4}$$

Equation (A4) can be rewritten as:

$$\begin{aligned}&\left\{1+\sum_{x=1}^{n}(G_{\mathrm{vd}x}(s)f_{cx}(s))\right\}\frac{\sum_{x=1}^{n}(I_x)}{G_{\mathrm{iv}}(s)}\\&=\sum_{x=1}^{n}\{G_{\mathrm{vd}x}(s)G_{\mathrm{ic}x}(s)(I_{\mathrm{r}x}-I_x)\}\end{aligned} \tag{A5}$$

In fact, (A5) can be reformulated as follows:

$$\begin{aligned}&\left\{1+\sum_{x=1}^{n}(G_{\mathrm{vd}x}(s)f_{cx}(s))\right\}\sum_{x=1}^{n}(I_x)\\&=G_{\mathrm{iv}}(s)\sum_{x=1}^{n}\{G_{\mathrm{vd}x}(s)G_{\mathrm{ic}x}(s)(I_{\mathrm{r}x}-I_x)\}\end{aligned} \tag{A6}$$

Then, by combing similar terms, (A7) can be given as follows:

$$\begin{aligned}&\left\{1+\sum_{x=1}^{n}(G_{\mathrm{vd}x}(s)f_{cx}(s))\right\}\sum_{x=1}^{n}(I_x)\\&\quad+G_{\mathrm{iv}}(s)\sum_{x=1}^{n}\{G_{\mathrm{vd}x}(s)G_{\mathrm{ic}x}(s)I_x\}\\&=G_{\mathrm{iv}}(s)\sum_{x=1}^{n}\{G_{\mathrm{vd}x}(s)G_{\mathrm{ic}x}(s)I_{\mathrm{r}x}\}\end{aligned} \tag{A7}$$

Although (A7) seems to be a multi-input multi-output system, it can actually be written as multiple single-input single-output systems, as shown in (A8).

$$\begin{aligned}&\left\{\left\{1+\sum_{x=1}^{n}(G_{\mathrm{vd}x}(s)f_{cx}(s))\right\}+G_{\mathrm{iv}}(s)G_{\mathrm{vd}k}(s)G_{\mathrm{ic}k}(s)\right\}I_k\\&=G_{\mathrm{iv}}(s)G_{\mathrm{vd}x}(s)G_{\mathrm{ic}x}(s)I_{\mathrm{r}k}\end{aligned} \tag{A8}$$

Then, closed-loop transfer function $G_{\mathrm{iifc}k}(s)$ of current control of k^{th} LRC can be obtained, as shown in (A9).

$$G_{\mathrm{iifc}k}(s)=\frac{I_{\mathrm{r}k}}{I_k}=\frac{G_{\mathrm{vd}k}(s)G_{\mathrm{ic}k}(s)G_{\mathrm{iv}}(s)}{\left\{\begin{array}{c}1+\sum_{x=1}^{n}(G_{\mathrm{vd}x}(s)f_{cx}(s))\\+G_{\mathrm{vd}k}(s)G_{\mathrm{ic}k}(s)G_{\mathrm{iv}}(s)\end{array}\right\}} \tag{A9}$$

B. Detailed Deduction of Voltage Control Transfer Function

Considering state feedback control, current and voltage control, duty $D_k(s)$ of k^{th} LRC can be written as follows:

$$D_k(s)=\{G_{\mathrm{ic}k}(s)\{G_{\mathrm{ic}k}(s)(V_{\mathrm{ref}k}-V)-I_k\}-f_{ck}(s)V\} \tag{B1}$$

Taking (B1) into consideration, (A1) can be rewritten as:

$$\begin{aligned}V=&\sum_{x=1}^{n}\{G_{\mathrm{vd}x}(s)G_{\mathrm{ic}x}(s)\{G_{\mathrm{vc}x}(s)(V_{\mathrm{ref}x}-V)-I_x\}\\&-G_{\mathrm{vd}x}(s)f_{cx}(s)V\}\end{aligned} \tag{B2}$$

By combining similar terms for (B2), the following equation can be obtained.

$$\begin{aligned}&V+\sum_{x=1}^{n}\{G_{\mathrm{vd}x}(s)G_{\mathrm{ic}x}(s)\{G_{\mathrm{vc}x}(s)V+I_x\}\\&\quad+G_{\mathrm{vd}x}(s)f_{cx}(s)V\}\\&=\sum_{x=1}^{n}(G_{\mathrm{vd}x}(s)G_{\mathrm{ic}x}(s)G_{\mathrm{vc}x}(s)V_{\mathrm{ref}x})\end{aligned} \tag{B3}$$

Similarly, (B3) can be reformulated as follows:

$$\begin{aligned}&\left\{\sum_{x=1}^{n}\{G_{\mathrm{vd}x}(s)G_{\mathrm{ic}x}(s)(G_{\mathrm{vc}x}(s)+p_xG_{\mathrm{iv}}(s))\}\right.\\&\quad\left.+\sum_{x=1}^{n}\{G_{\mathrm{vd}x}(s)f_{cx}(s)\}+1\right\}V\\&=\sum_{x=1}^{n}(G_{\mathrm{vd}x}(s)G_{\mathrm{ic}x}(s)G_{\mathrm{vc}x}(s)V_{\mathrm{ref}x})\end{aligned} \tag{B4}$$

Obviously, (B4) can be seen as a multi-input single-output system. Therefore, closed-loop transfer function $G_{\mathrm{vivfc}k}(s)$ of voltage control of k^{th} LRC can be obtained, as shown in (B5).

$$G_{\mathrm{vivfc}k}(s) = \frac{V_{\mathrm{ref}x}}{V} = \frac{G_{\mathrm{vd}x}(s)G_{\mathrm{ic}x}(s)G_{\mathrm{vc}x}(s)}{\left\{\begin{array}{c}\sum_{x=1}^{n}\{G_{\mathrm{vd}x}(s)G_{\mathrm{ic}x}(s)(G_{\mathrm{vc}x}(s)+p_xG_{\mathrm{iv}}(s))\}\\ +\sum_{x=1}^{n}\{G_{\mathrm{vd}x}(s)f_{\mathrm{c}x}(s)\}+1\end{array}\right\}} \tag{B5}$$

C. Detailed Deduction of Droop Control Transfer Function

Taking state feedback control, current control, voltage control and droop control into account, duty $D_k(s)$ of k^{th} LRC can be given as follows:

$$\begin{aligned} D_k(s) = \{&G_{\mathrm{ic}k}(s)G_{\mathrm{vc}k}(s)(V_{\mathrm{ref}k} - V_{\mathrm{r}k}(s) - V) \\ &- G_{\mathrm{ic}k}(s)G_{\mathrm{vc}k}(s)I_k - f_{\mathrm{c}k}(s)V\} \end{aligned} \tag{C1}$$

Combining (C1) to (A1), multi-converters MVDC power system can be rewritten as:

$$\begin{aligned} V = \sum_{x=1}^{n}\{&G_{\mathrm{vd}x}(s)G_{\mathrm{ic}x}(s)G_{\mathrm{vc}x}(s)(V_{\mathrm{ref}x} - V_{\mathrm{r}x}(s) - V) \\ &- G_{\mathrm{vd}x}(s)[G_{\mathrm{ic}x}(s)G_{\mathrm{vc}x}(s)I_x + f_{\mathrm{c}x}(s)V]\} \end{aligned} \tag{C2}$$

Then, voltage closed-loop transfer function $G_{\mathrm{vivrfc}k}(s)$ of k^{th} LRC can be obtained, as shown in (C3).

$$G_{\mathrm{vivrfc}k}(s) = \frac{V_{\mathrm{ref}x}}{V} = \frac{G_{\mathrm{vd}x}(s)G_{\mathrm{ic}x}(s)G_{\mathrm{vc}x}(s)}{\left\{\begin{array}{c}\sum_{x=1}^{n}\{G_{\mathrm{vd}x}(s)G_{\mathrm{ic}x}(s)(G_{\mathrm{vc}x}(s)(1+rC_{\mathrm{eq}}s)\\ +p_xG_{\mathrm{iv}}(s))\}+\sum_{x=1}^{n}\{G_{\mathrm{vd}x}(s)f_{\mathrm{c}x}(s)\}+1\end{array}\right\}} \tag{C3}$$

REFERENCES

[1] T. Dragičević, X. N. Lu, J. C. Vasquez, and J. M. Guerrero, "DC microgrids—part I: a review of control strategies and stabilization techniques," *IEEE Transactions on Power Electronics*, vol. 31, no. 7, pp. 4876–4891, Jul. 2016.

[2] T. Dragičević, X. N. Lu, J. C. Vasquez, and J. M. Guerrero, "DC microgrids—part II: a review of power architectures, applications, and standardization issues," *IEEE Transactions on Power Electronics*, vol. 31, no. 5, pp. 3528–3549, May 2016.

[3] G. Sulligoi, D. Bosich, G. Giadrossi, L. Zhu, M. Cupelli, and A. Monti, "Multiconverter medium voltage DC power systems on ships: constant-power loads instability solution using linearization via state feedback control," *IEEE Transactions on Smart Grid*, vol. 5, no. 5, pp. 2543–2552, Sep. 2014.

[4] N. Hatziargyriou, J. Milanovic, C. Rahmann, V. Ajjarapu, C. Canizares, I. Erlich, D. Hill, I. Hiskens, I. Kamwa, B. Pal, P. Pourbeik, J. Sanchez-Gasca, A. Stankovic, T. V. Cutsem, V. Vittal, and C. Vournas, "Definition and classification of power system stability – revisited & extended," *IEEE Transactions on Power Systems*, vol. 36, no. 4, pp. 3271–3281, Jul. 2021.

[5] H. Yuan, X. M. Yuan, and J. B. Hu, "Modeling of grid-connected VSCs for power system small-signal stability analysis in DC-link voltage control timescale," *IEEE Transactions on Power Systems*, vol. 32, no. 5, pp. 3981–3991, Sep. 2017.

[6] N. Rashidirad, M. Hamzeh, K. Sheshyekani, and E. Afjei, "High-frequency oscillations and their leading causes in DC microgrids," *IEEE Transactions on Energy Conversion*, vol. 32, no. 4, pp. 1479–1491, Dec. 2017.

[7] P. P. Pan, W. Chen, L. C. Shu, H. Mu, K. Zhang, M. Zhu, and F. J. Deng, "An impedance-based stability assessment methodology for DC distribution power system with multivoltage levels," *IEEE Transactions on Power Electronics*, vol. 35, no. 4, pp. 4033–4047, Apr. 2020.

[8] X. Chen, J. Y. Zhou, M. X. Shi, L. F. Yan, W. P. Zuo, and J. Y. Wen, "A novel virtual resistor and capacitor droop control for HESS in medium-voltage DC system," *IEEE Transactions on Power Systems*, vol. 34, no. 4, pp. 2518–2527, Jul. 2019.

[9] Q. W. Xu, X. L. Hu, P. Wang, J. F. Xiao, P. F. Tu, C. Y. Wen, and M. Y. Lee, "A decentralized dynamic power sharing strategy for hybrid energy storage system in autonomous DC microgrid," *IEEE Transactions on Industrial Electronics*, vol. 64, no. 7, pp. 5930–5941, Jul. 2017.

[10] J. W. Chen and Q. C. Song, "A decentralized energy management strategy for a fuel cell/supercapacitor-based auxiliary power unit of a more electric aircraft," *IEEE Transactions on Industrial Electronics*, vol. 66, no. 7, pp. 5736–5747, Jul. 2019.

[11] Y. H. Huang and D. Wang, "Effect of control-loops interactions on power stability limits of VSC integrated to AC system," *IEEE Transactions on Power Delivery*, vol. 33, no. 1, pp. 301–310, Feb. 2018.

[12] P. F. Lin, C. L. Zhang, P. Wang, and J. F. Xiao, "A decentralized composite controller for unified voltage control with global system large-signal stability in DC microgrids," *IEEE Transactions on Smart Grid*, vol. 10, no. 5, pp. 5075–5091, Sep. 2019.

[13] W. T. Jiang, X. N. Zhang, F. H. Guo, J. W. Chen, P. Wang, and L. H. Koh, "Large-signal stability of interleave boost converter system with constant power load using sliding-mode control," *IEEE Transactions on Industrial Electronics*, vol. 67, no. 11, pp. 9450–9459, Nov. 2020.

[14] Y. H. Huang, D. Wang, L. Shang, G. R. Zhu, H. Y. Tang, and Y. Li, "Modeling and stability analysis of DC-link voltage control in multi-VSCs with integrated to weak grid," *IEEE Transactions on Energy Conversion*, vol. 32, no. 3, pp. 1127–1138, Sep. 2017.

[15] J. B. Hu, H. Yuan, and X. M. Yuan, "Modeling of DFIG-based WTs for small-signal stability analysis in DVC timescale in power electronized power systems," *IEEE Transactions on Energy Conversion*, vol. 32, no. 3, pp. 1151–1165, Sep. 2017.

[16] J. Sun, M. C. Xu, M. Cespedes, and M. Kauffman, "Data center power system stability — part I: power supply impedance modeling," *CSEE Journal of Power and Energy Systems*, vol. 8, no. 2, pp. 403–419, Mar. 2022.

[17] J. Sun, M. Mihret, M. Cespedes, D. Wong, and M. Kauffman, "Data center power system stability — part II: system modeling and analysis," *CSEE Journal of Power and Energy Systems*, vol. 8, no. 2, pp. 420–438, Mar. 2022.

[18] Y. F. Li, G. F. Tang, J. Ge, Z. Y. He, H. Pang, J. Yang, and Y. N. Wu, "Modeling and damping control of modular multilevel converter based DC grid," *IEEE Transactions on Power Systems*, vol. 33, no. 1, pp. 723–735, Jan. 2018.

[19] L. Guo, P. F. Li, X. L. Li, F. Gao, D. Huang, and C. S. Wang, "Reduced-order modeling and dynamic stability analysis of MTDC systems in DC voltage control timescale," *CSEE Journal of Power and Energy Systems*, vol. 6, no. 3, pp. 591–600, Sep. 2020.

[20] P. F. Li, L. Guo, X. L. Li, H. D. Wang, L. Zhu, F. Gao, J. B. Zhu, and C. S. Wang, "Reduced-order modeling and comparative dynamic analysis of DC voltage control in DC microgrids under different droop methods," *IEEE Transactions on Energy Conversion*, vol. 36, no. 4, pp. 3317–3333, Dec. 2021.

[21] N. Rashidirad, M. Hamzeh, K. Sheshyekani, and E. Afjei, "A simplified equivalent model for the analysis of low-frequency stability of multi-bus DC microgrids," *IEEE Transactions on Smart Grid*, vol. 9, no. 6, pp. 6170–6182, Nov. 2018.

[22] F. Gao, S. Bozhko, A. Costabeber, G. Asher, and P. Wheeler, "Control design and voltage stability analysis of a droop-controlled electrical power system for more electric aircraft," *IEEE Transactions on Industrial Electronics*, vol. 64, no. 12, pp. 9271–9281, Dec. 2017.

[23] Q. W. Xu, Y. D. Yan, C. L. Zhang, T. Dragicevic, and F. Blaabjerg, "An offset-free composite model predictive control strategy for DC/DC buck converter feeding constant power loads," *IEEE Transactions on Power Electronics*, vol. 35, no. 5, pp. 5331–5342, May 2020.

[24] C. L. Zhang, X. Y. Wang, P. F. Lin, P. X. Liu, Y. D. Yan, and J. Yang, "Finite-time feedforward decoupling and precise decentralized control for DC microgrids towards large-signal stability," *IEEE Transactions on Smart Grid*, vol. 11, no. 1, pp. 391–402, Jan. 2020.

Xueshen Zhao received the B.S. and M.S. degrees in Electrical Engineering from Shandong University of Technology, Shandong, China, in 2016 and 2019, respectively. His research interests include stability analysis and optimal control of DC distribution system.

Lin Zhu received the B.S. and M.S. degrees from China Agriculture University, Beijing, China, in 2008 and 2010, respectively, and the Ph.D. degree from RWTH Aachen University, Aachen, Germany, in 2018, all in Electrical Engineering. Since 2010, she has been a Research Associate with the Institute of Automation of Complex Power Systems, E.ON Energy Research Center, Aachen, Germany. Since 2019, she has been a Lecturer with the School of Electrical Engineering and Automation, Tianjin University, Tianjin, China. Her research interests include stability analysis, control and hardware in the loop simulation in DC, and hybrid AC/DC power systems.

Li Guo received B.S. and Ph.D. degrees in Electrical Engineering from South China University of Technology in 2002 and 2007, respectively. Dr. Guo is currently a full Professor at Tianjin University. His research interests include the optimal planning and design of microgrid, and the advanced energy management system.

Xialin Li received the B.S. and Ph.D. degrees from Tianjin University, Tianjin, China, in 2009 and 2014, respectively. Since 2014, he has been a Lecturer with the School of Electrical Engineering and Automation, Tianjin University, China. His current research interests include the modeling and control of power converters.

Zhi Wang received the B.Sc. and M.Sc. degrees in Electrical Engineering from Tianjin University, Tianjin, China, in 2020 and 2023, respectively. He is currently working toward the Ph.D. degree in Electrical Engineering at Tianjin University, Tianjin, China. His current research interests include modeling, stability analysis and control of power electronics dominated power systems.

Hao Lu received the B.S. degree in Electrical Engineering from Tianjin University, Tianjin, China, in 2020. He is currently working toward the M.E. degree at Tianjin University. His research interests include stability analysis, control in DC power system.

Chengshan Wang received the Ph.D. degree in Electrical Engineering from Tianjin University, Tianjin, China, in 1991. From 1994 to 1996, he was a Senior Academic Visitor with Cornell University, Ithaca, NY, USA. From 2001 to 2002, he was a Visiting Professor with Carnegie Mellon University, Pittsburgh, PA, USA. He is currently a professor with the School of Electrical Engineering and Automation, Tianjin University, where he is also the Director of the Key Laboratory of Smart Grid of Ministry of Education. His current research interests include distribution system analysis and planning, distributed generation system and micro-grid, and power system security analysis.